The influence of viscous hydrodynamics on the fish lateral-line system

Shane P. Windsor[1]* and Matthew J. McHenry[†]

*School of Biological Sciences, University of Auckland, Auckland 1142, New Zealand; [†]Department of Ecology & Evolutionary Biology, University of California, Irvine, CA 92697, USA

Synopsis Fish exhibit many behaviors that involve sensing water flows with their lateral-line system. In many situations, viscosity affects how the flow interacts with the body of the fish and the neuromasts of the lateral line. Here we discuss how viscosity influences the stimulus to the fish lateral-line system. The movement of a fish's body creates flows that can interfere with the detection of external signals, but these flows can also serve as a source of information about nearby obstacles and the fish's own hydrodynamic performance. The viscous boundary layer on the surface of the skin alters external signals by attenuating the low-frequency components of stimuli. The stimulus to each neuromast depends on the interaction of the fluid surrounding the neuromast and the structural properties of that neuromast, including the number of mechanosensory hair cells it contains. A consideration of the influences of viscosity on flow, at both the whole-body and receptor levels, offers the promise of a more comprehensive understanding of the signals involved in behaviors mediated by the lateral-line system.

Introduction

Fish exhibit many behaviors that rely on their ability to sense water flow using their lateral-line system. When the lateral line system is experimentally disabled, fish showed impaired detection of prey (Liang et al., 1998; Coombs et al., 2001; Pohlmann et al., 2004), evasion of predators (Blaxter and Fuiman, 1989), avoidance of obstacles (Abdel-Latif et al., 1990; Hassan et al., 1992), mating (Satou et al., 1994), schooling (Pitcher et al., 1976; Partridge and Pitcher, 1980), and rheotaxis (Montgomery et al., 1997; Baker and Montgomery, 1999). This suggests that the lateral-line system is essential for the sensory ecology of fish, especially in conditions with minimal visual information (e.g. at night, in turbid waters, in caves, or in the deep sea). However, we have a limited knowledge of the hydrodynamic signals received by the lateral-line system and how fish use this information to guide specific behaviors. A major challenge to expanding our understanding of the lateral-line system lies in the complexity of viscous hydrodynamics, which influences both the flow patterns around the body and the micromechanics of the individual lateral-line receptors. Here we describe how viscous hydrodynamics influence the flow signals detected by the lateral-line system of fish.

Water flows can convey ecologically important information, but a variety of sources may interfere with the ability of fish to detect these signals. For example, some predatory fish locate prey from the flows generated by the motion of the prey (Coombs et al., 1989). This signal may be altered by flows created by the swimming motion of the predator or other currents in the environment (Fig. 1), to change the flow field over the surface of the body of the predator. Although it has been recognized that the viscosity of water can influence the stimulus to the lateral line (Jielof et al., 1952; Teyke, 1988; Kalmijn, 1989), viscous hydrodynamics are just beginning to be incorporated into our understanding of the lateral-line system. This oversight may partially be attributed to the complexity of the flows that are generated by a moving fish (Muller et al., 1997; Drucker and Lauder, 1999; Anderson et al., 2001), as these flows are difficult to model analytically. Despite this complexity, the general principles governing viscous hydrodynamics are well understood and their application to the lateral-line system is experimentally tractable. As we describe below, the relative simplicity of the flow field around a gliding fish provides an example of a behavior where the flow around a fish may be evaluated with flow visualization and computational

From the symposium "Sensory Biomechanics" presented at the annual meeting of the Society for Integrative and Comparative Biology, January 3–7, 2009, at Boston, Massachusetts.
[1]E-mail: shane.windsor@zoo.ox.ac.uk
Integrative and Comparative Biology, volume 49, number 6, pp. 691–701
doi:10.1093/icb/icp084
Advanced Access publication August 19, 2009

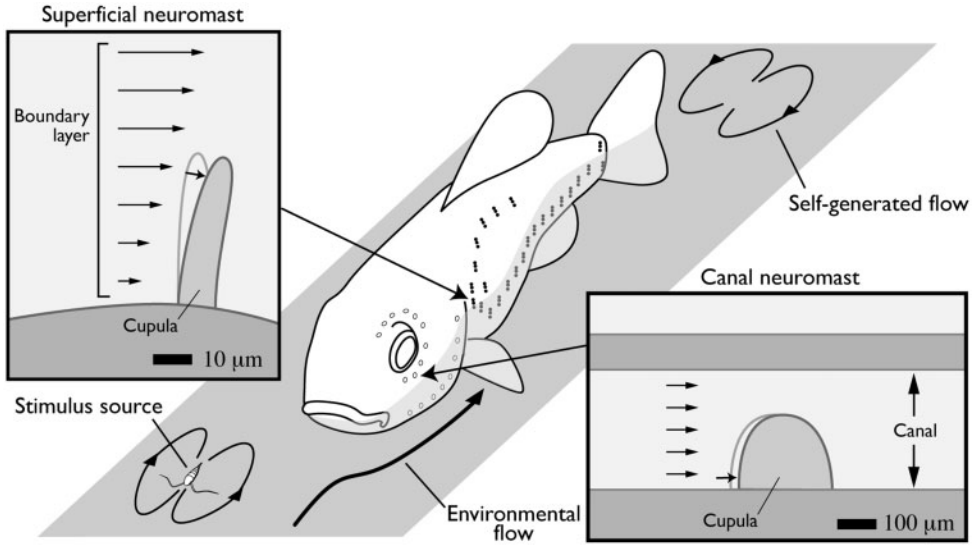

Fig. 1 Schematic of sources of flow stimuli for the lateral-line system. The superficial and canal neuromasts of the lateral-line system (insets) sense flow over the surface of the body. Superficial neuromasts are directly excited by the viscous boundary layer, whereas canal neuromasts detect flow within a canal beneath the skin. Both function by encoding the deflection of a gelatinous cupula. The detection of a flow stimulus, represented here as a copepod, may be complicated by interference from the flow generated by the movement of the fish and the ambient flow in the environment.

models to understand how self-motion can provide a signal for the detection of obstacles as well as a source of interference to other stimuli.

Flows around the body of a fish are detected by the hydrodynamic receptors of the lateral-line system (Fig. 1). These receptors, called neuromasts, include an extracellular cupula that extends into the water and is deflected by water flow. Cupular deflections cause the underlying apical ciliary bundles of hair cells to be displaced and these displacements are, in turn, transduced into electrical potentials. Canal neuromasts are located between pores inside fluid-filled canals under the skin. Neurophysiological, hydrodynamic, and biophysical lines of investigation agree that canal neuromasts are sensitive to pressure gradients over a broad range of stimulus frequencies (Coombs and van Netten, 2006; van Netten, 2006; Sane and McHenry, this volume). In contrast, superficial neuromasts are located on the surface of the skin and are directly excited by flow over the skin surface. As we discuss below, the morphology of a neuromast influences the sensing of flow through its effect on the fluid-structure interaction between the cupula and the surrounding water.

Flows around the body of a fish

Gliding provides a simple behavior for examining self-generated viscous flow. Many species of fish exhibit a glide phase during routine intermittent swimming, and this relatively inactive period between tail beats provides an opportunity for fish to sense stimuli in the flow around them (Fuiman and Webb, 1988). Few measurements have been made of the flow fields around gliding fish, but their general properties can be estimated from what is known about flows around other streamlined bodies, such as airfoils (Fig. 2). The flow around any body depends on the relative importance of inertia (fluid momentum) compared to viscosity (fluid friction), as quantified by the Reynolds number (*Re*).

$$Re = \frac{UL\rho}{\mu} \quad (1)$$

where U is velocity, L is the characteristic length (in this case the body length of the fish), and ρ and μ are the density and dynamic viscosity of the fluid respectively.

Flows around streamlined bodies are dominated by inertia at high Reynolds numbers ($Re > 100{,}000$), and may be thought of as being made up of a far field flow and a boundary layer flow on the body surface. The far field (potential) component of the flow is created by the body displacing the fluid through which it is moving, and it is not affected by viscosity. The displacement of the fluid around the body creates a pressure gradient along the body. In the frame of reference of the body, there is a point at the tip of the nose where the water is stationary (a stagnation point), creating a region of

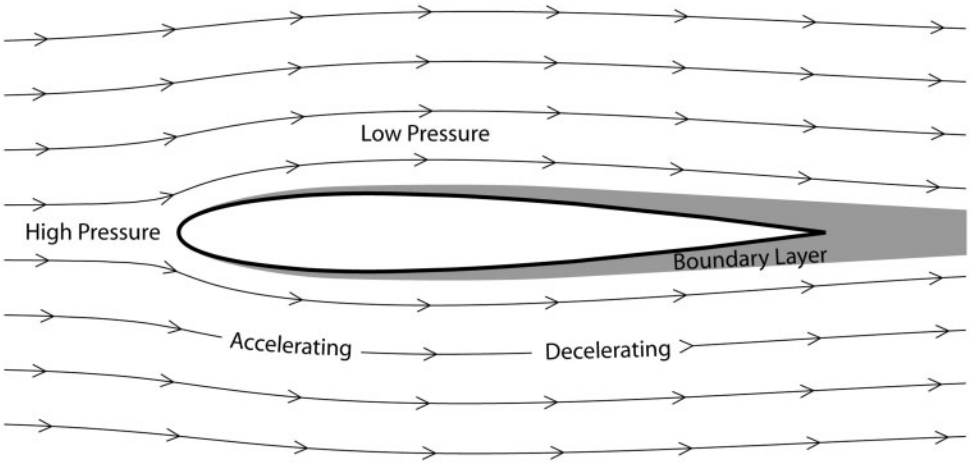

Fig. 2 Streamlines representing the general form of the flow field around a gliding fish or other streamlined body. The high pressure region at the nose corresponds to a stagnation point, the low pressure region around the widest part of the body corresponds to where the flow is accelerating around the body. On the surface of the body a thickening boundary layer forms due to viscous frictional forces.

high pressure. The water then accelerates from this point, around the body until reaching the widest part of the body, creating a low pressure region. The water then decelerates as it moves along the remaining length of the body. Very close to the surface of the body, there is a thin layer of fluid where the velocity changes from that of the body to that of the free-stream; this is known as the viscous boundary layer and it grows in thickness along the body. This is the result of the water, which is in direct contact with the body surface, adhering to the body and acting to progressively slow water further from the body through viscous frictional forces. The thickness of the boundary layer is conventionally defined as the distance away from a surface at which the velocity achieves a magnitude equal to 99% of the free-stream velocity. Most fish swim at Reynolds numbers ($\sim 100 < Re < \sim 100{,}000$) at which these two components of the flow field can still be detected, but at which they influence each other to a much greater extent due to viscous interactions than in flows at higher Reynolds numbers. Due to this close coupling, what is known about flows at higher Reynolds numbers is not directly applicable at lower Reynolds numbers and it is necessary to consider the increasingly important effect of viscosity.

Superficial neuromasts have been considered to respond in proportion to the velocity of the flow surrounding them (Kroese et al., 1978; Kalmijn, 1988; Kalmijn, 1989). However, this definition is simplistic because superficial neuromasts within the viscous boundary layer encounter a range of velocities that vary with the distance from the surface of the skin. A more accurate approximation of the stimulus for the superficial neuromasts is provided by the wall shear stress (τ_w) on the surface of the skin.

$$\tau_w = \mu \left(\frac{\partial u}{\partial y} \right) \Bigg|_{y=0} \quad (2)$$

where u is the tangential velocity and y is the direction normal to the surface.

Over a small gliding fish experimental measurements and computational fluid dynamics (CFD) modeling (Fig. 3) show that the boundary layer is thin over the head of the fish, corresponding to a steep velocity gradient and therefore to a large shear stress and a greater stimulus to the superficial neuromasts (Windsor, 2008). This is due to the negative pressure gradient over the head, from the high pressure region at the nose to the low pressure region around the widest part of the fish, accelerating the flow along the body. Further along the body of the fish, where the pressure gradient reverses and becomes shallower, the boundary layer rapidly thickens, decreasing the tangential velocity gradient and the stimulus to the superficial neuromasts (Fig. 4A). The presence of these pressure gradients means that the growth boundary layer along the body is not well modeled as a flat plate with a zero pressure gradient. The thickness of the boundary layer decreases with increasing Reynolds number (Fig. 3C), and correspondingly, the shear stress and the stimulation to the superficial neuromasts increases.

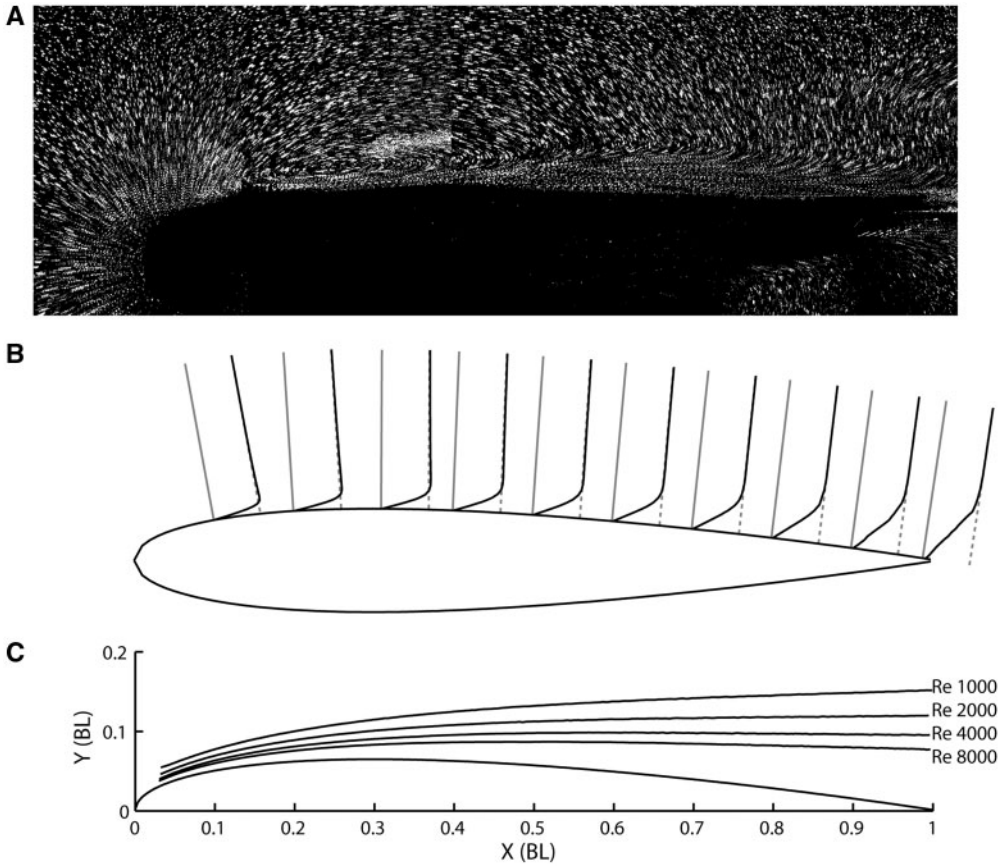

Fig. 3 Boundary layer over the surface of a gliding blind Mexican cave fish (*Astyanax mexicanus*) (Windsor, 2008). (A) Synthetic particle streak image over 25 ms from a PIV video sequence of a fish (length = 60 mm) viewed from a dorsal perspective at Re 6000. This image is composed of a montage of four separate images as the fish passed through the field of view. (B) CFD boundary layer velocity profiles of flow around a revolved 3D body based on a NACA 0013 aerofoil at Re 6000, showing the tangential velocity profile (black line), the zero tangential velocity axes normal to body surface (solid gray line), and the free-stream tangential velocity component relative to the body surface (dashed grey line). (C) CFD results of the effect of the Reynolds number on the 99% boundary layer profiles for a 2D NACA 0013 aerofoil. The same pattern was seen for the 3D body shown in B.

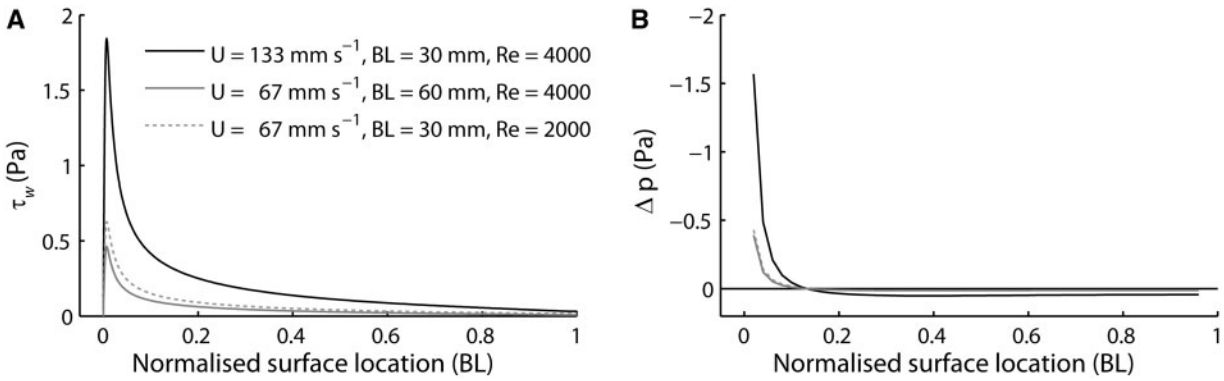

Fig. 4 CFD results of the effect of body length and velocity on the lateral line stimuli for a 2D NACA 0008 aerofoil (Windsor, 2008). Legend applies to both graphs. (A) Shear stress distributions along the length of the body of simulated fish of varying body length and swimming speed. (B) Pressure differences across pores at 2% body length (BL) spacing (note that the grey solid and dashed lines overlap). Consistent with the convention in aerodynamics, the *Y*-axis is reversed, so a negative pressure difference means a more positive pressure at the rostral pore. If these distributions were normalized by $0.5\rho U^2$ then distributions at the same Reynolds numbers would be identical.

The pressure across the thickness of a boundary layer can be accurately approximated as being constant (White, 2006). Therefore, the stimulus to the canal neuromasts is not directly filtered by the presence of the boundary layer as is the stimulus to the superficial neuromasts. However, at the Reynolds numbers at which most fish operate ($\sim 100 < Re < \sim 100{,}000$) the overall form of the flow field is strongly affected by viscosity, and the pressure gradient along the body is affected by the viscous interaction between the body and the surrounding flow. This is illustrated by the differences in the flow fields seen at high and low Reynolds numbers around airfoils (Lissaman, 1983; Huang and Lin, 1995; Kunz and Kroo, 2001; Mateescu and Abdo, 2004; Abdo, 2005).

The magnitude of the stimuli to both the superficial and canal neuromasts is determined more by the velocity of the fish than the body length of the fish. The pressure gradient is proportional to U^2 and the shear stress to $U^{1.5}$ (White, 2006). Assuming the body shape of the fish remains constant, a larger fish swimming at the same speed as a smaller fish will have nearly identical lateral-line stimulation, even though the Reynolds numbers will be quite different (Fig. 4). Conversely, a large fish and a smaller fish swimming at the same Reynolds number will have very different stimuli to their lateral lines. This is because the shear stress and pressure gradient fields do not scale directly with body length.

The flow field around a swimming fish is much more dynamic than the flow field around a gliding fish. Boundary layer measurements made using particle tracking velocimetry (PTV) (Anderson et al., 2001) show that the properties of the boundary layer oscillate with time and position along the surface of a swimming fish. The boundary layers observed ranged from fully laminar (smooth and steady) down the whole length of the body to fully turbulent (fluctuating and chaotic), depending on the Reynolds numbers involved and the level of background turbulence. In some cases the boundary layer appeared to oscillate between turbulent and laminar. Transition to a turbulent boundary layer could have a great effect on the stimuli to the superficial neuromasts as the flow varies chaotically over time, thereby producing a fluctuating stimulus to the superficial neuromasts. This stimulation would be dependent on the height of the cupula of the neuromast relative to the height of the laminar sub-layer of the turbulent boundary layer. The stimuli to the canal neuromasts would not be directly affected by the presence of the boundary layer as discussed previously. However, a large stimulus to the canal lateral line would be generated by the pressure oscillations that propagate along the body of a swimming fish (Wolfgang et al., 1999).

The superficial and canal lateral line will both be stimulated by the flow fields created by the motion of the fish. In the case of gliding, the pattern of the stimuli will be relatively constant, decreasing steadily in magnitude as the fish slows. When the fish is actively swimming the oscillations of the flow field will create stimuli that vary over time. In both of these cases, self-generated stimuli will make it more difficult for the fish to sense externally generated flows, but this will be a larger problem when actively swimming. For example, blind Mexican cave fish (*Astyanax mexicanus*) detect obstacles by sensing the changes the obstacles create in the flow field generated by the movement of the fish. These fish were found to collide with obstacles more frequently when they were beating their tail as they approached an obstacle than when they were gliding (Windsor et al., 2008). In a similar manner, stationary fish in a steady flow have reduced sensitivity to external sources of flow compared to when there is no background flow (Montgomery and Milton, 1993; Kanter and Coombs, 2003; Bassett et al., 2006).

The stimuli generated by the motion of a swimming fish may be used by the fish to modulate its motion. The separation of the boundary layer from the body surface increases the energetic costs associated with swimming. Boundary-layer separation around swimming fish was not seen by Anderson et al. (2001) even though velocity profiles that suggested the flow was close to separating were observed. This suggests that fish may act to avoid boundary layer separation. The superficial and canal neuromasts are suited to detect boundary-layer separation, as both will experience a change in the direction of stimuli at the point of separation. This suggests that hydrodynamic information from the flow field generated by swimming could be measured by the lateral line and be used to avoid boundary-layer separation by altering the motion of the body. However, this idea remains to be tested experimentally.

Neuromast micromechanics

Viscous hydrodynamics play a direct role in determining how flow is transformed into voltage potentials by a neuromast. The cupula of a canal or superficial neuromast (Fig. 5) encounters a drag force that is proportional to flow velocity (van Netten and Kroese, 1987). This causes the cupula to deflect to a degree that depends on its stiffness

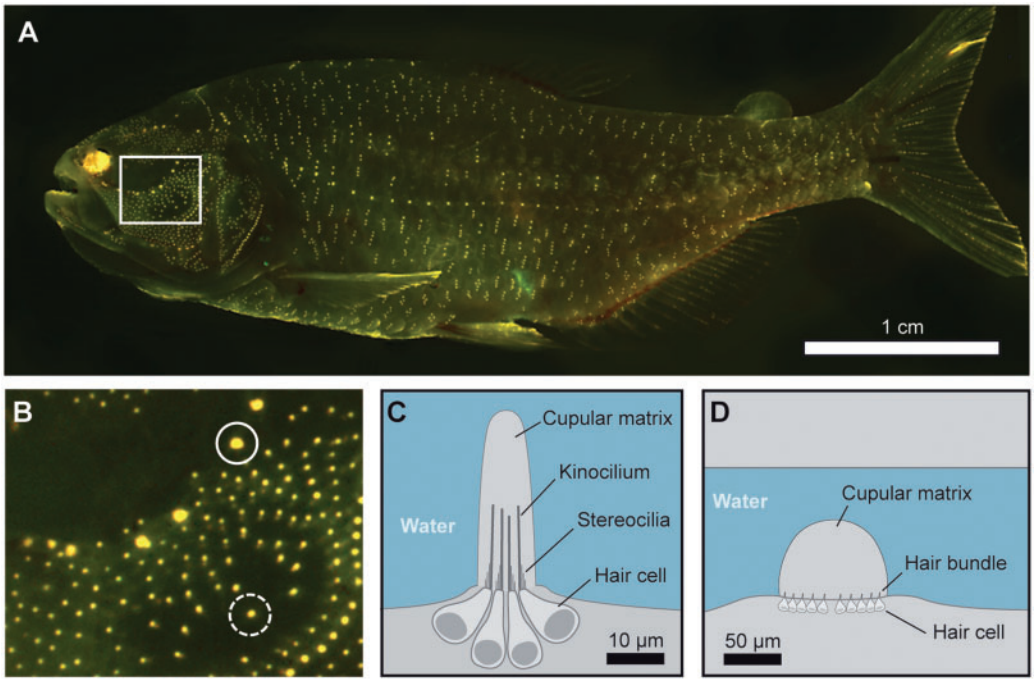

Fig. 5 The structure of superficial and canal neuromasts. (A) Individual neuromasts appear as yellow points due to fluorescent staining [2-(4-(dimethylamino)styryl)-*N*-ethylpyridinium iodide] of the hair cells in the blind Mexican cave fish (*Astyanax mexicanus*). A magnified view (white box) of (B) a portion of the head highlights the different sizes of canal (solid circle) and superficial (dashed circle) neuromasts. (C) A schematic of a superficial neuromast illustrates its main anatomical features. The kinocilium and stereocilia that comprise a hair bundle appear as a single line in (D), a schematic drawing of a canal neuromast.

and this deflection is transduced into nerve potentials by hair bundles within the gelatinous cupula. Each hair bundle consists of a kinocilium that is linked by structural proteins to a stair-step arrangement of microvilli, called stereocilia (Fig. 5C and D). As the hair bundle deflects, it loads mechanically-gated channels that alter the membrane potential of the hair cell. These graded potentials activate synapses to afferent neurons that transmit action potentials toward the central nervous system (Flock, 1965; Harris et al., 1970; Hudspeth, 1982).

Morphological differences between canal and superficial neuromasts create differences in how they detect water flow. When exposed to flow, the relatively large (hundreds of microns in diameter) and hemispherical cupula of a canal neuromast slides like a rigid body along the epilthelium. This deflection is resisted with spring-like dynamics by the hair bundles (van Netten and Kroese, 1987). Because of the viscous drag acting on the cupula, its deflections are proportional to the velocity of flow within the canal. This velocity is, in turn, proportional to pressure difference between the pores of the canal (van Netten, 2006). Although these dynamics change at higher frequencies due to cupular resonance and thinning of the boundary layer within the canal, the cupula and canal together cause a canal neuromast to be sensitive to the gradient of pressure over a broad range of stimulus frequencies (van Netten, 2006). This signal is detected without interference from the boundary layer on the skin surface (Rapo et al., 2009). It is consequently possible in some cases to predict the receptor potentials of canal neuromast hair cells from a potential flow model of pressure gradients around the body (see below).

In contrast to canal neuromasts, the ability of a superficial neuromast to detect flow is governed by the hydrodynamics of the boundary layer. As described above, a boundary layer developing from unidirectional flow attenuates the velocity of the flow close to the surface of the skin to a greater degree as the thickness of the boundary layer increases along the body. It is therefore anticipated that the boundary layer would create a greater degree of interference for superficial neuromasts in the posterior regions of a gliding fish. A stimulus may similarly be attenuated by an oscillating boundary layer. Instead of developing along the length of the body, the thickness of an oscillating boundary layer varies with frequency (Schlichting and Kestin, 1979). For example, the amplitude of velocity of flow at the height of a

superficial neuromast (e.g. 40 μm in zebrafish) (Van Trump and McHenry, 2008) is equal to ~2/3 of the amplitude of the free-stream flow when the free-stream flow is oscillating at 100 Hz (Fig. 7A). This ratio of velocities reduces to ~1/3 at 10 Hz, and to ~1/10 at 1 Hz. Therefore, flow close to the surface is attenuated by the boundary layer to a greater degree for low-frequency stimuli. In terms of signal processing, the boundary layer functions as a 'high pass' filter for superficial neuromasts because the high-frequency components of flow velocity are preferentially transmitted to the surface of the body.

Modeling how a superficial neuromast detects flow is complicated by the fluid-structure interaction between the cupula and the boundary layer (Fig. 6). Drag on the cupula depends on the velocity of flow relative to the cupula, but the rate of cupular deflection also depends on the drag. This coupling between drag and deflection necessitates a simultaneous consideration of both the beam dynamics and the hydrodynamics of the flow around the cupula to model the deflections that generate a neural signal. An analytical model of this fluid-structure interaction (Fig. 7) uses a combination of low-deflection beam theory, classic hydrodynamics for a cylinder, and boundary-layer dynamics for pressure-driven oscillatory flow (McHenry et al., 2008). This model calculates the mechanical sensitivity of a neuromast as the ratio of deflection of the cupula at the height of the tips of the stereocilia, (the site of mechano-transduction) (Hudspeth, 1982) to the free-stream velocity of flow. The model predictions can be used to interpret how the hydrodynamics and the structure of the cupula influence mechanical sensitivity over a range of stimulus frequencies. The change in the mechanical sensitivity of the

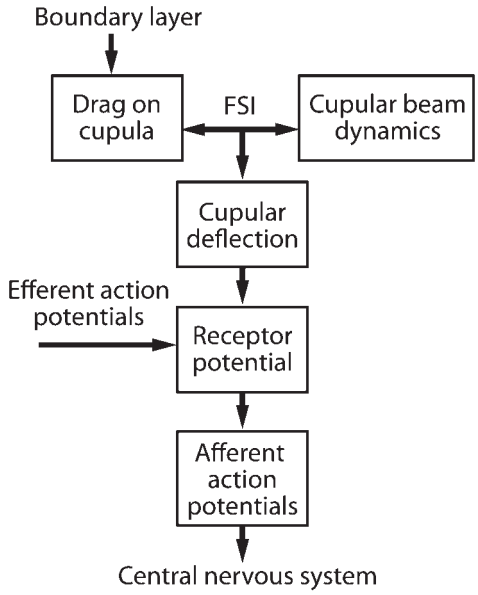

Fig. 6 A flow chart of the major components that factor into the sensing of boundary layer flow by a superficial neuromast. The flow chart illustrates how the fluid–structure interaction (FSI) between the drag generated by the boundary layer and the beam dynamics of the cupula generates deflections that are transduced by the hair cells into a receptor potential. The receptor potential may be modulated by efferent action potentials and leads to the generation of afferent action potentials that are processed by the central nervous system.

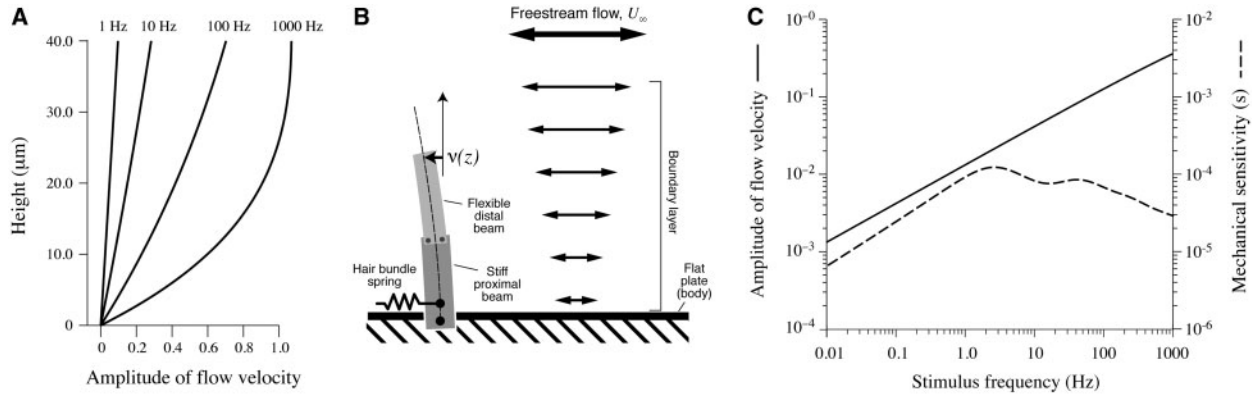

Fig. 7 Mechanical filtering within an oscillating boundary layer. The classic hydrodynamic model of the boundary layer generated over a flat plate in an oscillating pressure field demonstrates how the viscosity of water attenuates low frequency stimuli. In these graphs, the amplitude of the velocity of the flow was calculated as the ratio of velocity close to the plate to the free-stream velocity. (A) This amplitude increases with stimulus frequency at the height scale of a superficial neuromast. (B) A schematic of the FSI mechanics of a superficial neuromast that includes the boundary layer, a two-part beam model of the cupula, its coupling to the hair bundles, and the resulting deflection ν at a height z from the body's surface. (C) This model predicts an increase in mechanical sensitivity that occurs at a rate of 10 dB dec^{-1} at the height of the tips of the stereocilia (5.2 μm). These results are based on an adaptation of classic hydrodynamic theory (Batchelor, 1967; McHenry et al., 2008).

neuromast with frequency shows how the oscillating boundary layer acts like a high-pass filter. At low frequencies, the cupula is viscously coupled to the water and therefore deflects in proportion to the flow velocity close to the surface of the body (McHenry et al., 2008). However, this surface velocity increases with frequency at a rate of 10 dB dec^{-1} (solid line in Fig. 7C) because of the smaller influence of viscosity at higher frequencies. As a consequence, mechanical sensitivity (dashed line in Fig. 7C) shows a similar trend as the sensitivity of the boundary layer (solid line, Fig. 7C) at these low frequencies. Therefore, low frequency attenuation in the mechanical sensitivity of the neuromast is generated by the boundary layer.

The fluid-structure interaction of the cupula is affected by the number of hair cells within a neuromast. McHenry and van Netten (2007) found a positive correlation between the number of hair cells and the flexural stiffness of the cupula of superficial neuromasts in zebrafish larvae (solid line in Fig. 8A). This result arises from the high flexural stiffness of kinocilia relative to the cupular matrix. A single kinocilium was found to have a flexural stiffness (2.4×10^{-21} N m^2) that is more than one-third that of the entire cupular matrix (6.9×10^{-21} N m^2). Since superficial neuromasts typically possess between 4 and 15 hair cells (Van Trump and McHenry, 2008), the flexural stiffness of the proximal portion of the cupula is dominated by the kinocilia. Therefore, a neuromast possessing a greater number of hair cells is stiffer and consequently deflects less under drag than does a neuromast with fewer hair cells. This is reflected in the predictions of the mathematical model of superficial neuromast mechanics, which shows a monotonic decrease in mechanical sensitivity with a greater number of hair cells (dashed line in Fig. 8A).

The number of hair cells within a neuromast correlates with behavioral responses of larval fish to flow. When exposed to the impulsive flow of a feeding predatory fish, zebrafish larvae exhibit an escape response (McHenry et al., 2009). This response diminishes when the lateral-line hair cells are pharmacologically ablated, which suggests that this behavioral response is mediated by the lateral-line system. Furthermore, the ability to respond to flow recovers as the hair cells regenerate (Fig. 8B). Within the first day of recovery, the probability of an escape response is tightly correlated with the mean number of hair cells within each neuromast. This relationship may be due to an increase in the strength of the afferent signal created by more hair cells as they regenerate. Furthermore, the level of behavioral

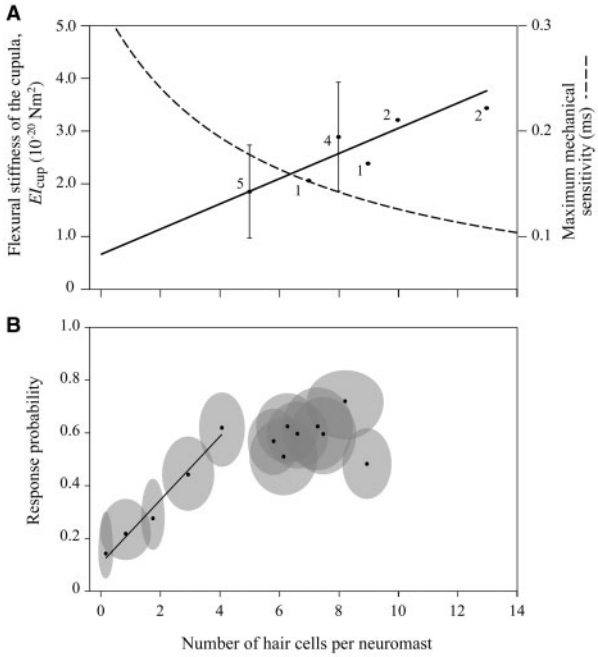

Fig. 8 The effects of hair cell number on superficial neuromast mechanics and behavior in zebrafish larvae. (A) The flexural stiffness of a superficial neuromast is proportional to the number of hair cells (solid line). Numbers indicate the number of measurements for each point (mean ± 1 SD) (McHenry and van Netten, 2007). The greater flexural stiffness that accompanies more hair cells causes a reduction in the mechanical sensitivity (the ratio of deflection at the tips of the stereocilia to the free-stream velocity, dashed line) in a mathematical model of cupular mechanics (McHenry et al., 2008). (B) The reduction in mechanical sensitivity may be a contributing factor in the lack of increase in response probability with greater hair cell numbers above four hair cells per neuromast. Response probability is the probability that a larva exhibits an escape response when exposed to a flow stimulus (areas denote 95% confidence intervals) (McHenry et al., 2009).

sensitivity maintained beyond four hair cells per neuromast (Fig. 8B) could be due to the reduced mechanical sensitivity that accompanies greater hair cell numbers. Alternatively, these behavioral changes may be caused by neurophysiological alterations that are independent of neuromast sensitivity. To distinguish between these hypotheses, one could perform experiments that measure how response probability varies with the intensity of the flow stimulus during the regeneration period. Characterizing the input-output function for behavior in this manner offers the potential to relate a behavioral response to stimuli detected by the superficial neuromasts.

When viscosity matters

There are some behaviors for which viscosity does not play a large role in the signals detected by the

lateral-line system. For example, a vibrating sphere approximates a prey animal well enough that some predators will strike at it in the dark (Coombs and Conley, 1997a). Using potential flow theory that negates viscosity, Coombs et al. (1996) modeled the flow field of a vibrating sphere as a dipole. They found that the calculated pressure gradients correlated with the spike rate of afferent neurons thought to innervate canal neuromasts. Additional results consistent with this interpretation have been reported for afferent neurons (van Netten and Kroese, 1987; Coombs and Conley, 1997b) and the microphonic potentials produced by the hair cells of canal neuromasts (Curcic-Blake and van Netten, 2006). Although viscous hydrodynamics are essential to how a canal neuromast detects flow within a canal (van Netten and Kroese, 1987), these results demonstrate that pressure gradients may be accurately modeled using only inviscid hydrodynamic theory under certain conditions (Rapo et al., 2009).

Although inviscid hydrodynamic theory remains valuable for studying the neurophysiology of canal neuromasts, this approach is limited in its ability to develop a broad understanding of the lateral-line system. Inviscid models do not predict boundary layers and therefore cannot be used to calculate the signals detected by superficial neuromasts. In order to model the boundary layer created by a vibrating sphere, van Netten (2006) developed a model that considered both viscous and inertial forces (based on Stokes, 1851). Using this model the response of superficial neuromasts was shown to vary substantially with small differences in the diameter of the sphere and its location with respect to the body because of large spatial variation in the velocity of the flow (McHenry et al., 2009). This complexity makes it more difficult for an investigator to interpret the signals received by the superficial neuromasts in response to a vibrating sphere than for canal neuromasts in the same situation. For example, the frequency response of afferent neurons of canal neuromasts to a vibrating sphere (Kroese and Schellart, 1992) match the pressure gradient predicted by hydrodynamic theory (Stokes, 1851; Harris and Vanbergeijk, 1962; Kalmijn, 1988; Sane and McHenry, this volume). However, the frequency responses attributed to superficial neuromasts in response to the same stimulus (Kroese et al., 1978; Kroese and Schellart, 1992) do not match the shape of the frequency response curves predicted by mechanical theory (McHenry et al., 2008). Simpler flows, such as a linear pressure field, would provide a stimulus that is easier to model and produce neuronal signals that are more tractable for studying superficial neuromasts than those generated by a vibrating sphere.

To fully understand the response properties of neuromasts, the local flow at the level of the receptor and the electrophysiological response of the receptor should be considered simultaneously. The use of flow measurement techniques such as particle image velocimetry (PIV) to measure flow in electrophysiological studies is providing new insights into the detection of spatial patterns of flow by the lateral line (e.g. Chagnaud et al., 2007a; Chagnaud et al., 2007b; Chagnaud et al., 2008). Techniques such as PIV can provide insight into the range of flow fields experienced by fish in their natural habitat and how these flows are influenced by interactions with the body of the fish. For example, these techniques have been used to characterize boundary-layer flows around swimming fish (Anderson et al., 2001) and local flows around fins (Coombs et al., 2007). Alternatively, physical models have been employed in previous work to assess the response of lateral-line like structures to different flow fields (e.g. Denton and Gray, 1983; Denton and Gray, 1988; Denton and Gray, 1989). With recent advances in artificial sensors that mimic the neuromasts of the lateral line (Fan et al., 2002; Yang et al., 2006), there is great potential to use physical models in experiments that are not possible with actual fish. For example, physical models could be used to study the effects of changing different aspects of the morphology of the canals, or altering the morphology and mechanical properties of the cupula of superficial neuromasts.

Summary

Viscosity affects lateral-line function by influencing both the flow around the body of a fish and the dynamics of individual neuromasts. Pressure gradients and viscous boundary layers form along the body of a fish due to gliding and swimming motions. These flows can interfere with the detection of external signals, but can also serve as a source of information about nearby obstacles and the fish's own hydrodynamic performance. Furthermore, viscous drag dominates the fluid-structure interactions that give rise to the neurobiological signal encoded by lateral-line neuromasts. Therefore, a comprehensive understanding of the signals received by the lateral-line system requires knowledge of how flows are affected by viscosity at both the whole-body and receptor levels. This knowledge will aid in understanding the signals involved in lateral-line mediated behaviors such as mating, schooling,

rheotaxis, detection of prey, evasion of predators, and avoidance of obstacles.

Funding

The Sensory Biomechanics Symposium at the 2009 Annual Meeting for the Society for Integrative & Comparative Biology was generously supported by Fastec Imaging, the Journal of Experimental Biology, the Company of Biologists, and the National Science Foundation (NSF, IOS-0904 089). Additional support was provided by the Divisions of Comparative Biomechanics, Vertebrate Morphology, and Neurobiology. MJM's research was supported by grants from the NSF (IOS-0723 288 and IOB-0509 740).

Acknowledgments

W.J. Van Trump contributed the photos of *Astyanax mexicanus*.

References

Abdel-Latif H, Hassan ES, von Campenhausen C. 1990. Sensory performance of blind Mexican cave fish after destruction of the canal neuromasts. Naturwissenschaften 77:237–9.

Abdo M. 2005. Low-Reynolds number aerodynamics of airfoils at incidence. Proceedings of the 3rd AIAA Aerospace Sciences Meeting and Exhibit. Reno, Nevada: American Instituite of Aeronautics and Astronautics.

Anderson EJ, McGillis WR, Grosenbaugh MA. 2001. The boundary layer of swimming fish. J Exp Biol 204:81–102.

Baker CF, Montgomery JC. 1999. The sensory basis of rheotaxis in the blind Mexican cave fish, *Astyanax fasciatus*. J Comp Physiol A 184:519–27.

Bassett DK, Carton AG, Montgomery JC. 2006. Flowing water decreases hydrodynamic signal detection in a fish with an epidermal lateral-line system. Mar Freshw Res 57:611–7.

Batchelor GK. 1967. An introduction to fluid dynamics. Cambridge: Cambridge University Press.

Blaxter JHS, Fuiman LA. 1989. Function of the free neuromasts of marine teleost larvae. In: Coombs S, Gorner P, Munz H, editors. The mechanosensory lateral line: neurobiology and evolution. New York: Springer-Verlag. p. 481–500.

Chagnaud BP, Bleckmann H, Hofmann MH. 2007a. Karman vortex street detection by the lateral line. J Comp Physiol A 193:753–63.

Chagnaud BP, Bleckmann H, Hofmann MH. 2008. Lateral line nerve fibers do not code bulk water flow direction in turbulent flow. Zoology 111:204–17.

Chagnaud BP, Hofmann MH, Mogdans J. 2007b. Responses to dipole stimuli of anterior lateral line nerve fibres in goldfish, *Carassius auratus*, under still and running water conditions. J Comp Physiol A 193:249–63.

Coombs S, Anderson E, Braun CB, Grosenbaugh M. 2007. The hydrodynamic footprint of a benthic, sedentary fish in unidirectional flow. J Acoust Soc Am 122:1227–37.

Coombs S, Braun CB, Donovan B. 2001. The orienting response of Lake Michigan mottled sculpin is mediated by canal neuromasts. J Exp Biol 204:337–48.

Coombs S, Conley RA. 1997a. Dipole source localization by mottled sculpin. 1. Approach strategies. J Comp Physiol A 180:387–99.

Coombs S, Conley RA. 1997b. Dipole source localization by the mottled sculpin. 2. The role of lateral line excitation patterns. J Comp Physiol A 180:401–15.

Coombs S, Gorner P, Munz H. 1989. The mechanosensory lateral line: neurobiology and evolution. New York: Springer-Verlag.

Coombs S, Hastings M, Finneran J. 1996. Modeling and measuring lateral line excitation patterns to changing dipole source locations. J Comp Physiol A 178:359–71.

Coombs S, van Netten SM. 2006. The hydrodynamics and structural mechanics of the lateral line system. In: Shadwick R, Lauder GV, editors. Fish biomechanics. New York: Elsevier. p. 103–39.

Curcic-Blake B, van Netten SM. 2006. Source location encoding in the fish lateral line canal. J Exp Biol 209:1548–59.

Denton EJ, Gray J. 1983. Mechanical factors in the excitation of clupeid lateral lines. Proc R Soc Lond Ser B Biol Sci 218:1–26.

Denton EJ, Gray J. 1988. Mechanical factors in the excitation of the lateral line of fishes. In: Atema J, Fay RR, Popper AN, Tavolga WN, editors. Sensory biology of aquatic animals. New York: Springer-Verlag. p. 595–618.

Denton EJ, Gray J. 1989. Some observations of the forces acting on neuromasts in fish lateral line canals. In: Coombs S, Gorner P, Munz H, editors. The mechanosensory lateral line: neurobiology and evolution. New York: Springer-Verlag. p. 229–46.

Drucker EG, Lauder GV. 1999. Locomotor forces on a swimming fish: three-dimensional vortex wake dynamics quantified using digital particle image velocimetry. J Exp Biol 202:2393–412.

Fan Z, Chen J, Zou J, Bullen D, Liu C, Delcomyn F. 2002. Design and fabrication of artificial lateral line flow sensors. J Micromech Microeng 12:655–61.

Flock A. 1965. Electron microscopic and electrophysiological studies on the lateral-line canal organ. Acta Oto-Laryngol Suppl 199:1–90.

Fuiman LA, Webb PW. 1988. Ontogeny of routine swimming activity and performance in zebra danios (Teleostei, Cyprinidae). Anim Behav 36:250–61.

Harris GG, Frishkop Ls, Flock A. 1970. Receptor potentials from hair cells of lateral line. Science 167:76–9.

Harris GG, Vanbergeijk WA. 1962. Evidence that lateral-line organ responds to near-field displacements of sound sources in water. J Acoust Soc Am 34:1831–41.

Hassan ES, Abdel-Latif H, Biebricher R. 1992. Studies on the effects of Ca++ and Co++ on the swimming behavior

of the blind Mexican cave fish. J Comp Physiol A 171:413–9.

Huang RF, Lin CL. 1995. Vortex shedding and shear-layer instability of wing at low-Reynolds numbers. AIAA J 33:1398–403.

Hudspeth AJ. 1982. Extracellular current flow and the site of transduction by vertebrate hair-cells. J Neurosci 2:1–10.

Jielof R, Spoor A, Devries H. 1952. The microphonic activity of the lateral line. J Physiol Lond 116:137–57.

Kalmijn AJ. 1988. Hydrodynamic and acoustic field detection. In: Atema J, Fay RR, Popper AN, Tavolga WN, editors. Sensory biology of aquatic animals. New York: Springer-Verlag. p. 83–130.

Kalmijn AJ. 1989. Functional evolution of lateral line and inner ear sensory systems. In: Coombs S, Gorner P, Munz H, editors. The mechanosensory lateral line: neurobiology and evolution. New York: Springer-Verlag. p. 187–216.

Kanter MJ, Coombs S. 2003. Rheotaxis and prey detection in uniform currents by Lake Michigan mottled sculpin (*Cottus bairdi*). J Exp Biol 206:59–70.

Kroese ABA, Schellart NAM. 1992. Velocity-sensitive and acceleration-sensitive units in the trunk lateral line of the trout. J Neurophysiol 68:2212–21.

Kroese ABA, Vanderzalm JM, Vandenbercken J. 1978. Frequency-response of lateral-line organ of *Xenopus-laevis*. Pflugers Arch Eur J Physiol 375:167–75.

Kunz PJ, Kroo I. 2001. Analysis and design of airfoils for use at ultra-low Reynolds numbers. In: Mueller TJ, editor. Fixed and flapping wing aerodynamics for micro air vehicle applications. Reston, VA: American Institute of Aeronautics and Astronautics. p. 35–60.

Liang XF, Liu JK, Huang BY. 1998. The role of sense organs in the feeding behaviour of Chinese perch. J Fish Biol 52:1058–67.

Lissaman PBS. 1983. Low-Reynolds-number airfoils. Annu Rev Fluid Mech 15:223–39.

Mateescu D, Abdo M. 2004. Aerodynamic analysis of airfoils at very low Reynolds numbers. *AIAA Paper*; Reno, NV, USA.Reston, USA: American Institute of Aeronautics and Astronautics Inc. p. 6341–51.

McHenry MJ, Feitl KE, Strother JA, Van Trump WJ. 2009. Larval zebrafish rapidly sense the water flow of a predator's strike. Royal Society Biology Letters 5:477–97.

McHenry MJ, Strother JA, van Netten SM. 2008. Mechanical filtering by the boundary layer and fluid-structure interaction in the superficial neuromast of the fish lateral line system. J Comp Physiol A 194:795–810.

McHenry MJ, van Netten SM. 2007. The flexural stiffness of superficial neuromasts in the zebrafish (*Danio rerio*) lateral line. J Exp Biol 210:4244–53.

Montgomery JC, Baker CF, Carton AG. 1997. The lateral line can mediate rheotaxis in fish. Nature 389:960–3.

Montgomery JC, Milton RC. 1993. Use of the lateral-line for feeding in the torrentfish (*Cheimarrichthys fosteri*). N Z J Zool 20:121–5.

Muller UK, VandenHeuvel BLE, Stamhuis EJ, Videler JJ. 1997. Fish foot prints: Morphology and energetics of the wake behind a continuously swimming mullet (*Chelon labrosus risso*). J Exp Biol 200:2893–906.

Partridge BL, Pitcher TJ. 1980. The sensory basis of fish schools – relative roles of lateral line and vision. J Comp Physiol 135:315–25.

Pitcher TJ, Partridge BL, Wardle CS. 1976. Blind fish can school. Science 194:963–5.

Pohlmann K, Atema J, Breithaupt T. 2004. The importance of the lateral line in nocturnal predation of piscivorous catfish. J Exp Biol 207:2971–8.

Rapo MA, Jiang H, Grosenbaugh M, Coombs S. 2009. Using computational fluid dynamics to calculate the stimulus to the lateral line of a fish in still water. J Exp Biol 212:1494–505.

Sane S, McHenry MJ. 2009. The biomechanics of sensory organs. Proceedings of the Society for Integrative Biology, January 3–7 in Boston, MA (http://www.sicb.org/meetings/2009/).

Satou M, Takeuchi HA, Tanabe M, Kitamura S, Okumoto N, Iwata M, Nishii J. 1994. Behavioral and electrophysiological evidences that the lateral-line is involved in the inter-sexual vibrational communication of the Hime salmon (land-locked red salmon, *Oncorhynchus nerka*). J Comp Physiol A 174:539–49.

Schlichting H, Kestin J. 1979. Boundary-layer theory. 7th ed. New York; London: McGraw-Hill.

Stokes GG. 1851. On the effect of the internal friction of fluids on the motion of pendulums. Trans Camb Phil Soc 9:8–106.

Teyke T. 1988. Flow field, swimming velocity and boundary layer: Parameters which affect the stimulus for the lateral line organ in blind fish. J Comp Physiol A 163:53–61.

van Netten SM. 2006. Hydrodynamic detection by cupulae in a lateral line canal: functional relations between physics and physiology. Biol Cybern 94:67–85.

van Netten SM, Kroese ABA. 1987. Laser interferometric measurements on the dynamic behavior of the cupula in the fish lateral line. Hear Res 29:55–61.

Van Trump WJ, McHenry MJ. 2008. The morphology and mechanical sensitivity of lateral line receptors in zebrafish larvae (*Danio rerio*). J Exp Biol 211:2105–15.

White FM. 2006. Viscous fluid flow. 3rd ed. Boston: McGraw-Hill.

Windsor SP. 2008. Hydrodynamic imaging by blind Mexican cave fish. PhD Thesis. Auckland: University of Auckland.

Windsor SP, Tan D, Montgomery JC. 2008. Swimming kinematics and hydrodynamic imaging in the blind Mexican cave fish (*Astyanax fasciatus*). J Exp Biol 211:2950–9.

Wolfgang MJ, Anderson JM, Grosenbaugh MA, Yue DKP, Triantafyllou MS. 1999. Near-body flow dynamics in swimming fish. J Exp Biol 202:2303–27.

Yang YC, Chen J, Engel J, Pandya S, Chen NN, Tucker C, Coombs S, Jones DL, Liu C. 2006. Distant touch hydrodynamic imaging with an artificial lateral line. Proc Natl Acad Sci USA 103:1889–95.